RSC Advances

PAPER

View Article Online
View Journal | View Issue

Cite this: *RSC Adv.*, 2019, **9**, 31636

Graphene quantum dots mediated electron transfer in DNA base pairs†

Chang Liu, Linqing Guo, Biao Zhang and Liping Lu *

Graphene quantum dots (GQDs) were connected to $[Ru(bpy)_3]^{2+}$ to sense DNA-mediated charge transfer. Interaction between abasic site double stranded DNA (Abasic-DNA) and $[Ru(bpy)_3–GQD]^{2+}$ was investigated by absorption spectroscopy, gel electrophoresis, circular dichroism, and melting temperature measurements. The results indicate that $[Ru(bpy)_3–GQD]^{2+}$ could be intercalated into double stranded DNA. Using $[Ru(bpy)_3–GQD]^{2+}$ as a signal molecule, the charge transfer performance of DNA-intercalated $[Ru(bpy)_3–GQD]^{2+}$ was determined using electrochemical and electrochemiluminescence measurements. Various DNA types were immobilized on Au electrodes *via* Au–S bonds. Electrochemiluminescence and electrochemical measurements indicate that $[Ru(bpy)_3–GQD]^{2+}$ could enhance DNA-mediated charge transfer when intercalated into an abasic site of double stranded DNA. And comparing with $[Ru(bpy)_3]^{2+}$, it can be concluded that GQDs intercalate into the DNA duplex by acting as a base analog, thus enhancing DNA charge transfer. These findings suggest that the DNA–GQD structure could aid the development of molecular devices and electric drivers, and broaden the application of DNA charge transfer.

Received 17th July 2019
Accepted 26th September 2019

DOI: 10.1039/c9ra05481b

rsc.li/rsc-advances

1. Introduction

Graphene is a monolayer of carbon atoms with a dense honeycomb crystal structure that can be stacked into graphite. As an emerging material, graphene quantum dots/carbon dots has been widely used in biosensing.[1–9] Graphene quantum dots (GQDs) are small graphene fragments, which can be one layer thick. GQDs stacked on top of each other have a structure similar to the stacked base pairs of DNA.[10–13] Consecutive base pairs of DNA are stacked closely together, allowing the interaction of adjacent aromatic systems of DNA. Double stranded DNA (dsDNA) is capable of mediating charge transport through its π-stacked base pairs,[14,15] and graphene exhibits outstanding electrical conductivity.[16–18] For this reason, GQDs are well suited for monitoring charge transport (CT) in DNA.

In the past few decades, DNA CT has received significant interest from biologists, physicists and chemists.[14,19,20] The rapid development of electronic techniques has led to the miniaturization of electronic devices, and thus to the development of molecular electronics.[21,22] DNA is a good candidate for molecular devices because of its unique identifiability and self-assembly capability.[23] Recent investigations have shown that CT is of great significance in understanding the mechanisms of genetic damage and message transmission, and for exploring methods for gene therapy.

A method of injecting charge onto a DNA strand and for reporting the CT event is necessary for investigating DNA CT.[24–27] Many studies have shown that metal complexes are good probes of DNA CT.[28–30] Varying the metal ligands and DNA-binding features are important parameters for governing DNA-mediated electron transfer. In addition, ancillary ligands can influence the electrochemical or photophysical properties of these complexes.[31,32] Particularly effective examples are transition metal complexes, which can sensitively tune their electronic and electrochemical or luminescent properties upon interaction with duplex DNA.[33,34] Since the $[Ru(phen)_3]^{2+}$ complex was reported to be capable of recognizing DNA,[35–37] polypyridyl ruthenium complexes have been widely used as probes of DNA secondary structure.[38–41] For example, the ruthenium complexes $[Ru(bpy)_3]^{2+}$ and $[Ru(bpy)_2dppz]^{2+}$ have been used as DNA probes.[30,42,43] The use of non-natural base analogues will further our understanding of the effect of close interactions between bases on DNA CT. Many base analogues only slightly perturb the geometry and structure of the base stack, because they interact in a natural way with other bases and become part of the base stack.

In the current study, GQDs were tailored as ligands or base analogues to sense CT in DNA, with the aim of enhancing CT in DNA. $[Ru(bpy)_3]^{2+}$ was used as a bridge to connect DNA and GQDs. Absorption spectroscopy, circular dichroism (CD), and polyacrylamide gel electrophoresis were used to investigate the interaction between the $[Ru(bpy)_3–GQD]^{2+}$ complex and DNA

Key Laboratory of Beijing on Regional Air Pollution Control, Beijing University of Technology, Beijing 100124, China. E-mail: lipinglu@bjut.edu.cn

† Electronic supplementary information (ESI) available. See DOI: 10.1039/c9ra05481b

duplex. Electrochemical and electrochemiluminescence (ECL) results illustrate the advantages of GQDs as a base analogue for studying CT in DNA.

2. Experimental

2.1 Materials and reagents

NaCl, NaH_2PO_4, Na_2HPO_4, $K_3[Fe(CN)_6]$, $K_4[Fe(CN)_6]$ and KCl were purchased from Beijing Chemical Works (P. R. China). Tripropylamine (TPA) was purchased from TCI Inc. (Japan). 1-(3-Dimethylaminopropyl)-3-ethylcarbodiimide hydrochloride (EDC), 2,2′-bipyridine-4,4′-diamine [bpy$(NH_2)_2$] and *cis*-bis-(2,2′-bipyridine)dichlororuthenium(II) $[RuCl_2(bpy)_2]^{2+}$ were purchased from Sigma Chemical Co. Ltd. *N*-Hydroxysuccinimide (NHS) was purchased from Sinopharm Chemical Reagent Co. Ltd. GQDs were purchased from Nanjing XFNANO Materials Tech Co. Ltd. Other reagents were purchased from Beijing Dingguo Changsheng Biotechnology Co. Ltd. Ultrapure water was used throughout, and was obtained from a Millipore Water Milli-Q water purification system. All reagents were of analytical grade. Oligonucleotide sequences were synthesized and purified by Sangong Biotech Co. Ltd.

2.2 Apparatus and measurements

Fluorescence spectra were recorded on a Hitachi F-4600 fluorescence spectrophotometer. The excitation wavelength was set at 380 nm, and emission spectra were recorded with the wavelength range of 400–680 nm. The widths of the excitation and emission slits were 10 nm. Proton nuclear magnetic resonance (^{1}H NMR) spectra were recorded on a Varian-500 spectrometer. Ultraviolet-visible (UV-vis) spectra were recorded on a Shimadzu UV-2450 spectrophotometer. CD spectra were recorded on an Applied Photophysics Pistar π-180 CD spectrometer, and the wavelength range was 350–200 nm. Native polyacrylamide gel electrophoresis was performed with a mini-gel apparatus (DYY-7C, Beijing Liuyi Scientific Equipment Ltd, P. R. China) using 20% acrylamide gel, and imaged on a Bio-Rad Gel Doc XR+ Imaging System.

2.3 Synthesis of dsDNA

All DNA solutions were thoroughly deoxygenated with argon prior to annealing, and stored in phosphate buffer saline (PBS) (5 mM, 0.1 M NaCl, pH 7.4). Equimolar amounts of single-stranded DNA (ssDNA) were combined and annealed by heating to 90 °C and subsequently cooling to ambient temperature over 90 min, to form duplexes. Abasic site dsDNA (labeled as Abasic-DNA) was obtained by hybridizing ssDNA-1, ssDNA-2, and ssDNA-3, as shown in Table S1.† Well matched double stranded DNA (WM-DNA) was obtained by hybridizing ssDNA-1 and ssDNA-4, as shown in Table S1.† One base-mismatched double stranded DNA (MM-DNA) was obtained by hybridizing ssDNA-1 and ssDNA-5, as shown in Table S1.† DNA synthesis reactions were carried out in a Bio-RAD T100 Thermal Cycler. The base sequences of DNA used in this study were:

ssDNA: 5′-CTC GGG GGC GCC AGC GGC CCC GGC TGC ATG AGC T***G***C AAG TGC GTG CTG AGC TGA GGA TCC-3′

Abasic-DNA: 3′- GAG CCC CCG CGG TCG CCG GGG CCG ACG TAC TCG A◆G TTC ACG CAC GAC TCG ACT CCT AGG-5′

WM-DNA: 3′-GAG CCC CCG CGG TCG CCG GGG CCG ACG TAC TCG A***C***G TTC ACG CAC GAC TCG ACT CCT AGG-5′

MM-DNA: 3′-GAG CCC CCG CGG TCG CCG GGG CCG ACG TAC TCG A**A**G TTC ACG CAC GAC TCG ACT CCT AGG-5′

2.4 Synthesis of $[Ru(bpy)_2(bpy(NH_2)_2)]^{2+}$

The $[RuCl_2(bpy)_2 \cdot 2H_2O]^{2+}$ (1 mM, 0.52 g) and bpy$(NH_2)_2$ (1.5 mM, 0.279 g) were dissolved in 20 mL of ethylene glycol/water (v/v, 9 : 1) in a three-necked flask. The solution was heated at reflux (120 °C) for 6 h, yielding a dark red solution, which was subsequently cooled to room temperature. 20 mL of water was added, and the resulting solution was filtered to obtain a dark red filtrate. The solution was then poured into 300 mL of aqueous NH_4PF_6, forming an orange-yellow precipitate. The precipitate was filtered off, washed with water and then acetonitrile, and dried under vacuum. The crude orange-yellow product was purified by column chromatography on neutral alumina with acetonitrile/methylbenzene as the eluent. The solvent was removed by rotary evaporation yielding red crystals (423 mg, yield 60%). ^{1}H NMR confirmed that $[Ru(bpy)_2(bpy(NH_2)_2)]^{2+}$ was obtained (Fig. S-1†).

2.5 Synthesis of $[Ru(bpy)_2(bpy(NH_2)_2)$–GQD$]^{2+}$

0.1 M EDC (20 μL) and 0.1 M NHS (10 μL) were added into an aqueous dispersion of GQDs, to activate the carboxylic acid groups. $[Ru(bpy)_2(bpy(NH_2)_2)]^{2+}$ was then incubated in the GQD solution ($[Ru(bpy)_2(bpy(NH_2)_2)]^{2+}$ (10 μM) : GQDs (1 μg mL^{-1}) = 1 : 5 v/v) for 30 min in a shaker to produce $[Ru(bpy)_2(bpy(NH_2)_2)$–GQD$]^{2+}$ (labeled as $[Ru(bpy)_3$–GQD$]^{2+}$) (Fig. S-3†).

2.6 Incubation of $[Ru(bpy)_3$–GQD$]^{2+}$ and dsDNA

$[Ru(bpy)_3$–GQD$]^{2+}$ was gently stirred in a warm bath at 37 °C. Different amounts of 25 μM Abasic-DNA were then added to the solution, which was incubated for another 10 min. The product was labeled as Abasic-DNA–Ru-GQD.

2.7 Fabrication of DNA-modified electrodes for electrochemical and ECL detection

Before surface modification, the Au electrode was polished in a 0.05 μm alumina/water slurry, followed by successive sonication in ultrapure water, ethanol and ultrapure water. The electrode was then immersed in freshly prepared piranha solution (98% H_2SO_4 : 30% H_2O_2, 7 : 3 v/v) for 10 min. The treated electrode was then rinsed thoroughly with ultrapure water and dried in a stream of N_2.

Immobilization of DNA was accomplished by dropping 10 μL of 25 μM thiolated ssDNA-1 (ssDNA), Abasic-DNA, ferrocene labeled Abasic-DNA (Fc-DNA), MM-DNA, or WM-DNA on the pre-cleaned Au electrode, which were labeled as ssDNA/Au, Abasic-DNA/Au, Fc-DNA/Au, MM-DNA/Au, and WM-DNA/Au, respectively. The reaction was maintained for 16–24 h in a humid environment, to ensure the formation of a DNA monolayer on the Au electrode *via* thiol–Au bonds. And then 6-

hydroxy-1-hexanethiol (MCH) was used for backfilling by casting 10 μL of 1 mM MCH onto the surface of Au electrode and incubated for 40 min to block the remaining active sites. The resulting electrodes were rinsed thoroughly with 5 mM PBS (pH 7.4), before use in detection measurements.

2.8 Electrochemical and ECL detection

Electrochemical impedance spectroscopy (EIS) measurements were conducted in 5.0 mM $K_3[Fe(CN)_6]/K_4[Fe(CN)_6]$ with a frequency ranging from 1 to 10^5 Hz. Electrochemical signals of ferrocene were obtained by recording cyclic voltammetry (CV) curves in 0.1 M phosphate buffer (pH 7.4). ECL measurements were performed using a MPI-E electroluminescent analyzer (Xian, P. R. China) with a potential range of 0.4–1.4 V and a scan rate of 100 mV s^{-1}. The ECL intensity was detected in 0.1 M TPA (pH 7.4, 0.1 M PBS) (Scheme 1).

3. Results and discussion

3.1 UV-vis and fluorescence analyses of $[Ru(bpy)_3$–GQD$]^{2+}$ complex

Fluorescence emission spectra of aqueous solutions of GQDs, $[Ru(bpy)_2(bpy(NH_2)_2)]^{2+}$ and $[Ru(bpy)_3$–GQDs$]^{2+}$ are shown in Fig. 1A. The GQD solution exhibits a strong photoluminescence emission centered at *ca.* 378 nm (dark purple). In contrast, a photoluminescence emission band at *ca.* 447 nm is observed for $[Ru(bpy)_2(bpy(NH_2)_2)]^{2+}$ (dark blue). There is a significant decrease in the characteristic fluorescent intensity of $[Ru(bpy)_3$–GQDs$]^{2+}$ solution (dark green), when compared to that of the GQDs. The fluorescence intensity at *ca.* 447 nm disappears in comparison with pure $[Ru(bpy)_2(bpy(NH_2)_2)]^{2+}$. This result suggests that GQDs as ligands for $[Ru(bpy)_2(bpy(NH_2)_2)]^{2+}$ have a strong fluorescence quenching effect.[44–46] A blue-shift in emission band to around 361 nm is observed for the $[Ru(bpy)_3$–GQDs$]^{2+}$ compared to GQDs. The blue shift is attributed to coupling of the conjugated hexagonal rings of the GQDs and $[Ru(bpy)_2(bpy(NH_2)_2)]^{2+}$ functional groups.[47,48]

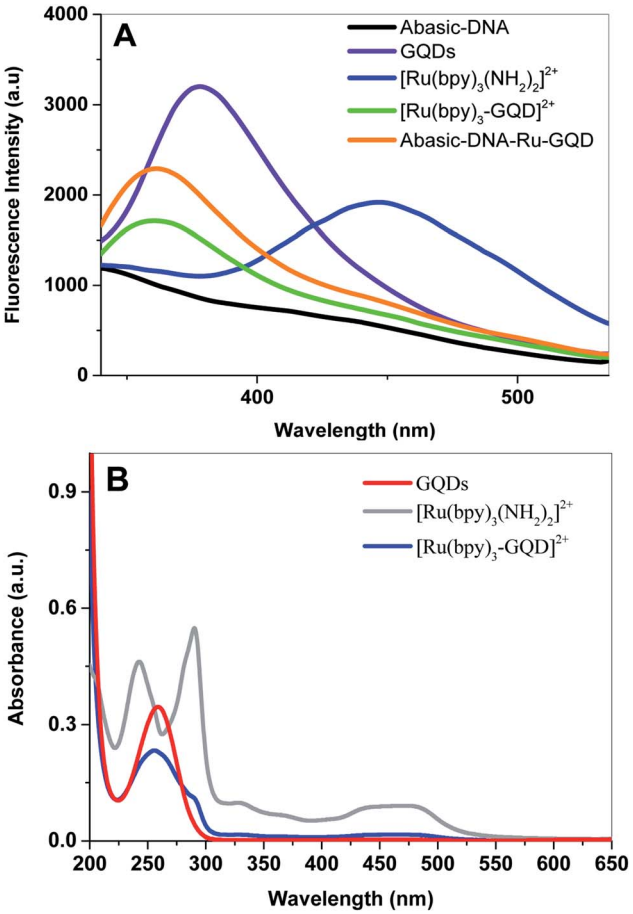

Fig. 1 (A) The fluorescence spectrum of Abasic-DNA (black), GQDs (dark purple), $[Ru(bpy)_2(bpy(NH_2)_2)]^{2+}$ (dark blue), $[Ru(bpy)_3$–GQD$]^{2+}$ complexes (dark green) and Abasic-DNA–Ru-GQD (saffron yellow). Ex = 280 nm. (B) UV-Vis absorption spectra of GQDs (red), $[Ru(bpy)_2(bpy(NH_2)_2)]^{2+}$ (silvery grey) and $[Ru(bpy)_3$–GQD$]^{2+}$ complexes (dark blue).

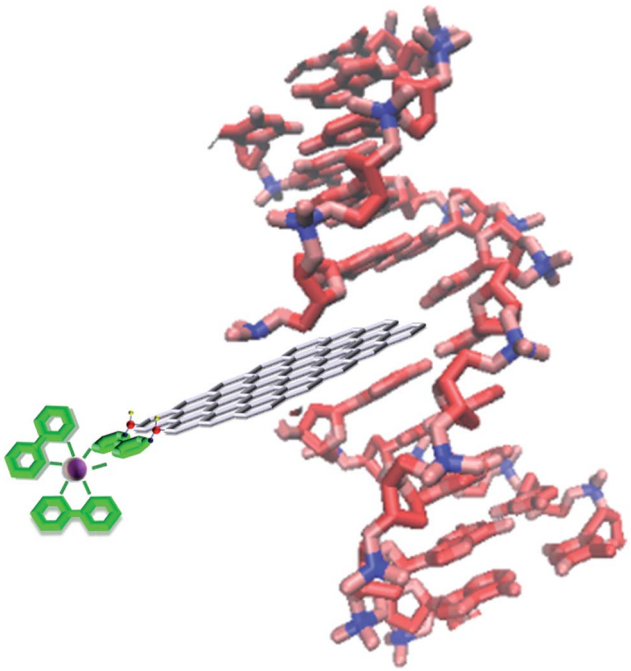

Scheme 1 The binding modes of $[Ru(bpy)_3$–GQD$]^{2+}$ with Abasic-DNA.

UV-vis absorption spectra of solutions containing $[Ru(bpy)_2(bpy(NH_2)_2)]^{2+}$, $[Ru(bpy)_3$–GQDs$]^{2+}$ and GQDs are shown in Fig. 1B. The GQD solution exhibits an absorption band at *ca.* 260 nm. Two strong absorption bands appear at *ca.* 240 nm and 280 nm, and a broad absorption appears at *ca.* 450 nm. These correspond to the π–π* transition and metal-to-ligand charge transfer (MLCT) adsorptions of $[Ru(bpy)_2(bpy(NH_2)_2)]^{2+}$.[49,50] When the GQDs are bound with $[Ru(bpy)_2(bpy(NH_2)_2)]^{2+}$, the π orbital of $[Ru(bpy)_2(bpy(NH_2)_2)]^{2+}$ can couple with the π orbital of the GQDs, with the coupled π orbital being partially filled with electrons. This decreases the energy of the π–π* transition, resulting in hypochromicity.[51] The absorption peak of $[Ru(bpy)_3$–GQD$]^{2+}$ is significantly red shifted compared with that of $[Ru(bpy)_2(bpy(NH_2)_2)]^{2+}$. This is

attributed to the significant decrease in HOMO–LUMO energy gap of $[Ru(bpy)_3–GQD]^{2+}$.[52]

3.2 Interaction between $[Ru(bpy)_3–GQD]^{2+}$ complex and Abasic-DNA

(1) UV-vis absorption and fluorescence analyses. UV-vis absorption spectroscopy is a simple and frequently used technique for studying interactions between DNA and small ligands.[53–55] It is especially useful for determining the interaction between Abasic-DNA and $[Ru(bpy)_3–GQD]^{2+}$. Specifically, the shifting of the band maximum of the free state of the ligand in solution upon binding with DNA can be observed. As shown in Fig. 2, $[Ru(bpy)_3–GQD]^{2+}$ and DNA have the same UV-vis absorption peak at 260 nm. The theoretical UV-vis absorption of Abasic-DNA–Ru-GQD is obtained from summing the data for $[Ru(bpy)_3–GQD]^{2+}$ and DNA (dotted curve, Fig. 2). Comparison with the UV-vis data for Abasic-DNA–Ru-GQD (blue curve, Fig. 2) shows evident hypochromism. This is consistent with the intercalation of a small molecule and DNA. This can decrease the distance of the stacking interaction between the GQD heterocycle and base pairs of DNA, thus decreasing the electronic interaction.[56] The same results are obtained from the fluorescence analysis. The Abasic-DNA–Ru-GQD shows a photoluminescence peak centered at *ca.* 361 nm, and shows much stronger photoluminescence emission than $[Ru(bpy)_3–GQD]^{2+}$ (Fig. 1A). The fluorescence enhancement could be attributed to the intercalation of GQDs into Abasic-DNA base pairs. This weakens molecular vibration by forming hydrogen bonds, and enhances photoluminescence emission. Comparing the photoluminescence of GQDs interacted with DNA and $[Ru(bpy)_2(bpy(NH_2)_2)]^{2+}$ interacted with DNA suggests that the GQDs interact with DNA preferentially to other ligands.

(2) Melting temperature and circular dichroism analyses. The intercalation of complexes into DNA base pairs can stabilize the base stacking.[57,58] The melting temperature (T_m) of DNA is defined as the temperature at which half of dsDNA is dissociated into single strands, and reflects the stability of the DNA macromolecule.[59] The intercalation of complexes into DNA base pairs increases the T_m of dsDNA, while non-intercalated binding does not enhance the T_m.[60] As shown in Fig. 3, the T_m of Abasic-DNA is 84.68 °C in the absence of $[Ru(bpy)_3–GQD]^{2+}$, and increases to 88.83 °C in the presence of $[Ru(bpy)_3–GQD]^{2+}$. The higher T_m indicates the enhanced stability of the DNA in the presence of $[Ru(bpy)_3–GQD]^{2+}$. The result supports the conclusion of intercalative binding of $[Ru(bpy)_3–GQD]^{2+}$ with Abasic-DNA.

Circular dichroism (CD) originates from interactions between chiral molecules and circularly polarized electromagnetic radiation. CD can be used to detect changes in DNA morphology. The band has a base stacking of 275 nm and a right-handed helicity of 248 nm, which make it sensitive to DNA interactions with small molecules.[61,62] CD spectra of Abasic-DNA (shown as Fig. S-2†) are characterized by a positive long wavelength band or bands at about 260–280 nm. These are due to base stacking. A negative band at around 250 nm results from the DNA helicity, and indicates a right-handed B-form helical conformation.[63–65] The conformation of Abasic-DNA changes after incubation with $[Ru(bpy)_3–GQD]^{2+}$ (shown as Fig. S-2†). The negative band at 247 nm is red shifted to 248 nm. The positive long wavelength band at 274 nm shifts to 272 nm. The results also indicate the interaction between $[Ru(bpy)_3–GQD]^{2+}$ and Abasic-DNA, which leads to a conformational change in Abasic-DNA.[66]

(3) Polyacrylamide gel electrophoresis of GQDs and dsDNA. The Abasic-DNA and Abasic-DNA–Ru-GQD complexes were studied for their electrophoretic mobility assay using polyacrylamide gel electrophoresis, and the results are shown in Fig. 4. Lanes 1, 2, 3 and 4 show the mobilities of Abasic-DNA, Abasic-DNA–GQD, Abasic-DNA–$[Ru(bpy)_2(bpy(NH_2)_2)]^{2+}$ and Abasic-DNA–Ru-GQD, respectively. The mobility of a charged species in electrophoresis depends on its charge and molecular weight. The molecular weight of each species in the four lanes is different. The results show that both Abasic-DNA–$[Ru(bpy)_2(bpy(NH_2)_2)]^{2+}$ and Abasic-DNA–Ru-GQD act on DNA, as that there are electrophoretic mobility differences when compared

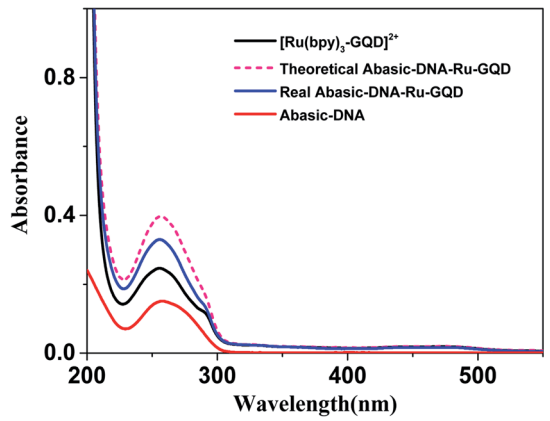

Fig. 2 UV-vis absorption spectrum of $[Ru(bpy)_3–GQD]^{2+}$ (black line), Abasic-DNA (red line), actual measured Abasic-DNA–Ru-GQD (dark blue line) and theoretical Abasic-DNA–Ru-GQD (pink dash line).

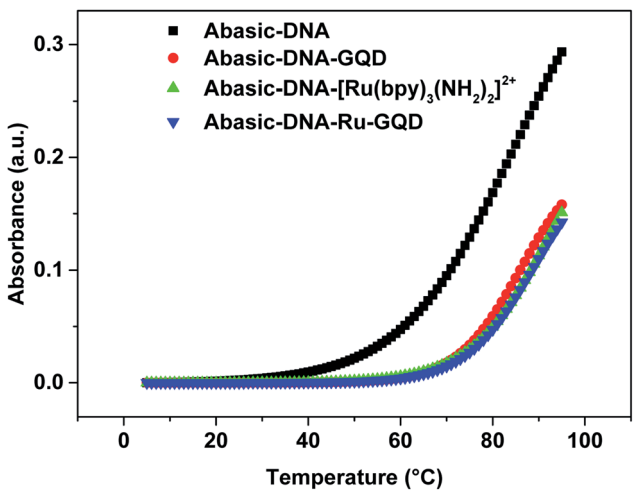

Fig. 3 Melting curves for Abasic-DNA and Abasic-DNA–Ru-GQD from the temperature dependence of CD at 260 nm.

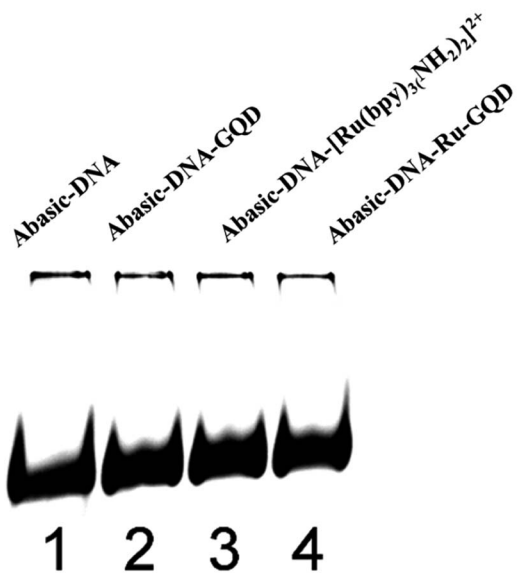

Fig. 4 Electrophoretic mobility of (lane 1) Abasic-DNA, (lane 2) Abasic-DNA–GQD, (lane 3): Abasic-DNA–$[Ru(bpy)_2(bpy(NH_2)_2)]^{2+}$, (lane 4) Abasic-DNA–Ru-GQD.

with the control DNA samples.[67] The band of Abasic-DNA–Ru-GQD in lane 4 lags behind that in lane 1. The difference in the positions of the bands is due to the successive decrease in the electrophoretic mobility of Abasic-DNA after binding with the Abasic-DNA–$[Ru(bpy)_2(bpy(NH_2)_2)]^{2+}$ and Abasic-DNA–Ru-GQD complexes. Abasic-DNA–Ru-GQD is heavier than Abasic-DNA. Thus, the electrophoretic mobility of Abasic-DNA–Ru-GQD is less than that of Abasic-DNA. For this reason, the Abasic-DNA–GQD band in lane 2 and Abasic-DNA–$[Ru(bpy)_2(bpy(NH_2)_2)]^{2+}$ band in lane 3 lag behind the Abasic-DNA band in lane 1, and are ahead of the Abasic-DNA–Ru-GQD band in lane 4.[68]

(4) Electrochemical analysis. Electrochemical methods are also useful for studying the interaction between metal chelates and DNA.[69] To further verify the binding mode of $[Ru(bpy)_3$–GQD$]^{2+}$ with DNA, CV curves were measured in the absence and presence of Abasic-DNA. Variations in peak potential and current reflect the effects of binding interactions.[70] As shown in Fig. 5A, $[Ru(bpy)_3$–GQD$]^{2+}$ has a cathodic peak at 0.44 V and an anodic peak at 0.90 V ($E_{1/2}$ = 0.67, refers as the average of E_{pa} and E_{pc}) in the absence of DNA, which are attributed to the redox process of the Ru^{2+}/Ru^{3+} couple.[71] The current decrease upon the addition of Abasic-DNA indicates the binding of Ru-GQD to DNA. Measurements of diffusion currents in the presence of excess nucleic acid have shown that DNA-bound species have much lower diffusion coefficients than free species.[72] Furthermore, the shift in peak potential to more positive values after adding Abasic-DNA is typical of species that intercalate into DNA.[73] CV curves of $[Ru(bpy)_3]^{2+}$ measured in the absence and presence of Abasic-DNA are shown in Fig. 5B. Similarly, the reduced current in the presence of DNA suggests the interaction between $[Ru(bpy)_3]^{2+}$ and DNA. The $E_{1/2}$ of the Abasic-DNA–$[Ru(bpy)_3]^{2+}$ adduct is 0.67 V, which is more negative than that

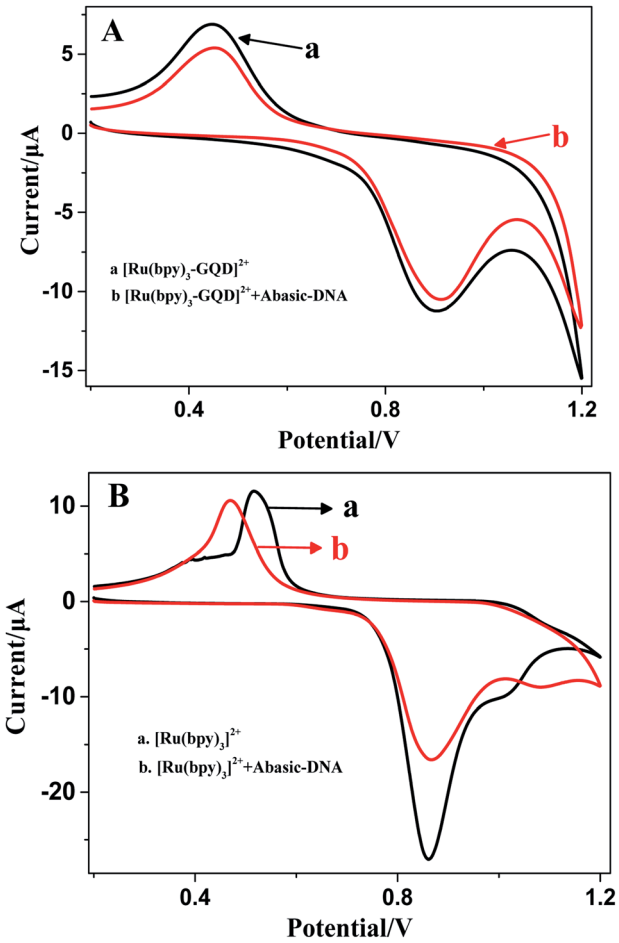

Fig. 5 Cyclic voltammograms of $[Ru(bpy)_3$–GQD$]^{2+}$ (A) and $[Ru(bpy)_3]^{2+}$ (B) in the absence (black line) and presence (red line) of Abasic-DNA.

of $[Ru(bpy)_3]^{2+}$ ($E_{1/2}$ = 0.70 V) as the result of electrostatic binding.[74]

3.3 Electron transfer assay

The Barton group has utilized transition metal complexes combined with DNA to mediate the CT response.[10,75] The current study investigates the use of metal complexes of $[Ru(bpy)_3$–GQD$]^{2+}$ as probes for initiating and monitoring DNA CT events by electrochemistry and ECL. The results have demonstrated the intercalation of $[Ru(bpy)_2(bpy(NH_2)_2)$–GQD$]^{2+}$ into Abasic-DNA. To investigate the performance of GQDs as a base, the CT of Abasic-DNA–Ru-GQD was studied using electrochemistry and ECL.

(1) EIS analysis. EIS can be used to study the surface features of modified electrodes using the redox probe $[Fe(CN)_6]^{3-/4-}$. EIS was used to investigate changes in the CT resistance (R_{ct}) resulting from each surface modification step, as shown in Fig. 6A. The EIS spectrum of the bare Au electrode shows a semicircle profile at high frequency, which is related to the electron-transfer-limited process, and a linear profile at lower frequency, which corresponds to diffusion. The increase in the

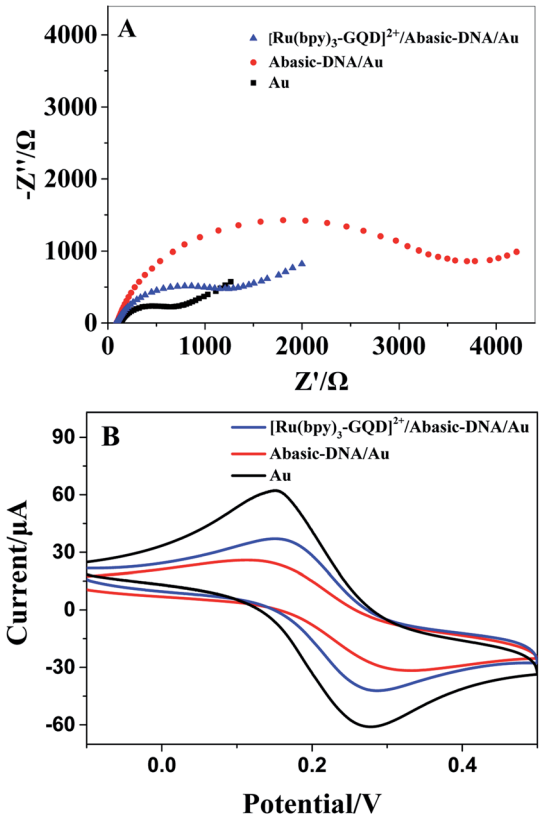

Fig. 6 (A) The EIS image of different modified electrodes. (B) The CV image of different modified electrodes.

diameter of the semicircle reflects the increase in interfacial R_{ct}.[76] Fig. 6A shows that the bare Au electrode exhibits an almost straight line at low frequencies corresponding to the diffusion process, and a very small semicircle at high frequencies. The R_{ct} is estimated to be about 600 Ω from the semicircle diameter. After the immobilization of thiolated Abasic-DNA, the R_{ct} increases from 600 Ω to 3500 Ω. This increase is due to the immobilization of negatively charged Abasic-DNA, which results in a negatively charged electrode surface. The surface then electrostatically repels the negatively charged redox probe $[Fe(CN)_6]^{3-/4-}$, and inhibits interfacial CT.[77] When $[Ru(bpy)_3$–$GQD]^{2+}$ is bound with Abasic-DNA, the R_{ct} decreases from 3500 Ω to 1300 Ω, because GQDs are intercalated into Abasic-DNA and mediate CT by acting as a base. $[Ru(bpy)_3$–$GQD]^{2+}$ is the intercalator and redox active species, and acts as a mediator to shuttle electrons along the DNA double helix.[78] CV can also probe the features of surface-modified electrodes. Fig. 6B shows that the redox peak current is enhanced when $[Ru(bpy)_3$–$GQD]^{2+}$ is intercalated into Abasic-DNA on the Au electrode. In summary, the EIS and CV results show that $[Ru(bpy)_3$–$GQD]^{2+}$ accelerates electron transfer in DNA.

(2) Electrochemical analysis. To further demonstrate the $[Ru(bpy)_3$–$GQD]^{2+}$-mediated DNA CT, ferrocenyl (Fc) was labeled onto the terminal of Abasic-DNA to investigate DNA CT.[79] Ferrocenyl has good reversible electrochemical performance. It also has faint redox performance on ferrocenyl-labelled Abasic-DNA/Au (black line in Fig. 7), because the abasic base attenuated CT of DNA for no perfect base stacked.

The ferrocenyl redox peak current is significantly increased in the presence of $[Ru(bpy)_3$–$GQD]^{2+}$ in solution (red line in Fig. 7). This result is attributed to the interaction of $[Ru(bpy)_3$–$GQD]^{2+}$ with Abasic-DNA, which forms ordered base stacking in the DNA duplex. It also promotes electron transfer between the DNA probe and electrode surface, because the GQDs have highly efficient electron transfer.[80,81] This further supports the conclusion that $[Ru(bpy)_3$–$GQD]^{2+}$ intercalated into Abasic-DNA acts as a base and mediates DNA CT.

(3) ECL analysis. Fig. 8A shows ECL-V curves for the four modified electrodes (ssDNA/Au, WM-DNA/Au, MM-DNA/Au and Abasic-DNA/Au). After immersing in $[Ru(bpy)_3$–$GQD]^{2+}$ solution for 10 min, the resulting electrodes were rinsed thoroughly with 5 mM PBS (pH 7.4), and then detected in 0.1 M TPA (pH 7.4, 0.1 M PBS). ssDNA/Au exhibits no ECL signal, since $[Ru(bpy)_3$–$GQD]^{2+}$ cannot be combined into ssDNA because of the lack of binding sites. There are obvious ECL signals for the other three dsDNA modified electrodes, which indicate the interaction of $[Ru(bpy)_3$–$GQD]^{2+}$ with dsDNA. A lower ECL intensity is obtained for MM-DNA/Au, since a base-mismatch can perturb CT compared to perfectly complementary WM-DNA.[82] Abasic-DNA has a higher ECL intensity than WM-DNA, confirming that the $[Ru(bpy)_3$–$GQD]^{2+}$ complex intercalates into the incomplete part of dsDNA, and replaces the absent base for more effective CT. Thus, thus the interaction between oxidized $[Ru(bpy)_3$–$GQD]^{2+}$ and TPA is increased, which enhances the ECL intensity.

The ECL response of $[Ru(bpy)_3]^{2+}$ (Fig. 8B) is distinctly different from that of $[Ru(bpy)_3$–$GQD]^{2+}$ on the dsDNA-modified electrodes. The interaction between $[Ru(bpy)_3]^{2+}$ and dsDNA is groove binding and electrostatic interaction.[83,84] Approximately the same ECL intensities are obtained for the MM-DNA/Au and WM-DNA/Au electrodes, and Abasic-DNA/Au has a slightly lower ECL intensity. This is because the absent base can disturb the formation of the duplex conformation and thus negatively affect CT.

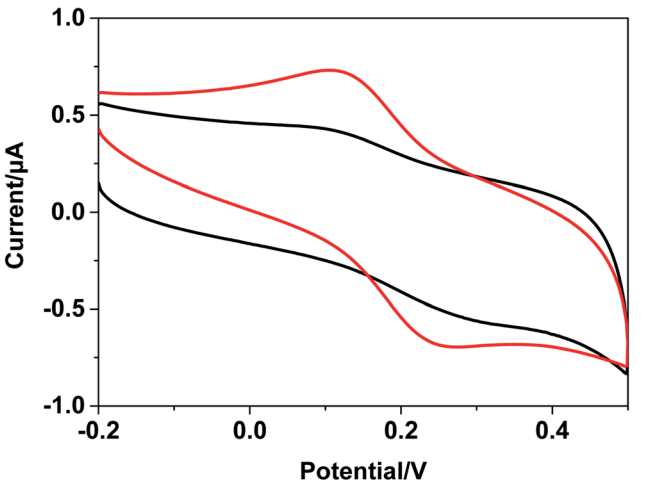

Fig. 7 Cyclic voltammograms with Fc-DNA/Au (black line) and $[Ru(bpy)_3$–$GQD]^{2+}$/Fc-DNA/Au (red line) in 0.1 M PBS.

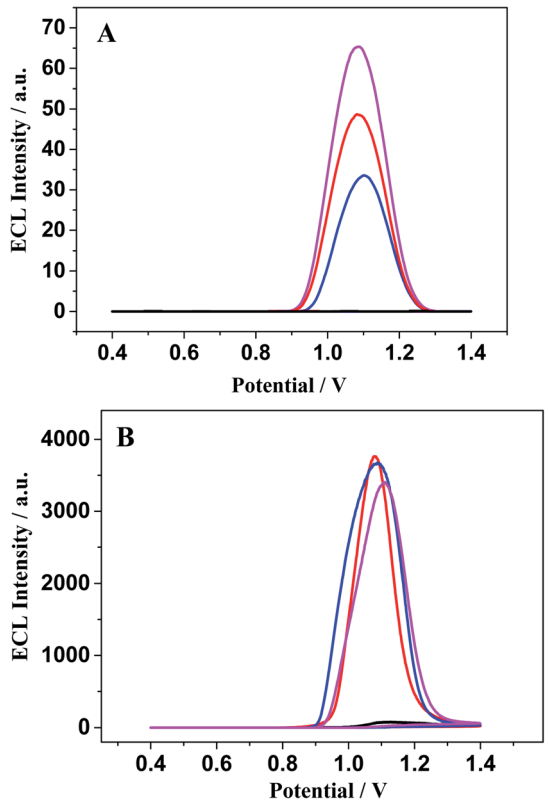

Fig. 8 The ECL signals of different modified electrode: ssDNA/Au (black), WM-DNA/Au (red), MM-DNA/Au (blue) and Abasic-DNA/Au (pink) immersed in $[Ru(bpy)_3–GQD]^{2+}$ (A) and $[Ru(bpy)_3]^{2+}$ (B) for 10 min before measurement. The detection was performed in 0.1 M PBS (pH 7.4) containing 0.1 M TPA.

4. Conclusions

In a word, We successfully synthesized the $[Ru(bpy)_2(bpy(NH_2)_2)]^{2+}$ and acquired $[Ru(bpy)_3–GQD]^{2+}$ complex through amide bond. The optical properties of complex were characterized by UV-vis and fluorescence techniques. Besides, We employed UV-vis absorption, fluorescence, melting temperature analyses as well as polyacrylamide gel electrophoresis techniques to further explore the interaction between $[Ru(bpy)_3–GQD]^{2+}$ and DNA duplex. Electrochemical and ECL analyses results indicated that abasic site domains could be substituted with GQDs, which Abasic-DNA was assembled on the Au electrode. Excitingly, the CT of the dsDNA was further enhanced in this way.

To the best of our knowledge, this is the first report about graphene quantum dots are connected with $[Ru(bpy)_3]^{2+}$ as a extended ligand. Graphene quantum dots were bound to $[Ru(bpy)_3]^{2+}$ as an ancillary ligand, which facilitated the binding of $[Ru(bpy)_3–GQD]^{2+}$ with single-base deleted dsDNA. In addition, this is also the first to demonstrate that graphene quantum dots could be intercalated into the DNA duplex by acting as a base analog, and enhancing DNA charge transfer. From the above, GQDs intercalated in DNA duplex possesses great potential in the development of biotechnology and biosensors.

Conflicts of interest

The authors declare no competing financial interest.

Acknowledgements

This work was financially supported by the National Natural Science Foundation of China (No. 21527808, 21876005) and Beijing Municipal High Level Innovative Team Building Program (IDHT 20180504).

References

1 H. Li, X. Wang, Z. Cai, L. Lu, J. Tao, B. Sun, Y. Yang, Q. Xu, Z. Yu and P. Zhao, *Anal. Bioanal. Chem.*, 2017, **409**, 6655–6662.
2 S. Lu, G. Xiao, L. Sui, T. Feng, X. Yong, S. Zhu, B. Li, Z. Liu, B. Zou, M. Jin, J. Tse, H. Yan and B. Yang, *Angew. Chem., Int. Ed.*, 2017, **56**, 6187–6191.
3 S. Lu, L. Sui, J. Liu, S. Zhu, A. Chen, M. Jin and B. Yang, *Adv. Mater.*, 2017, **29**, 1603443.
4 S. Tao, S. Lu, Y. Geng, S. Zhu, S. A. T. Redfern, Y. Song, T. Feng, W. Xu and B. Yang, *Angew. Chem., Int. Ed.*, 2018, **57**, 2393–2398.
5 S. Lu, L. Sui, M. Wu, S. Zhu, X. Yong and B. Yang, *Adv. Sci.*, 2019, **6**, 1801192.
6 Q. Wang, S. Zhang, B. Wang, X. Yang, B. Zou, B. Yang and S. Lu, *Nanoscale Horiz.*, 2019, **4**, 1227–1231.
7 W. Li, Y. Liu, M. Wu, X. Feng, S. A. T. Redfern, Y. Shang, X. Yong, T. Feng, K. Wu, Z. Liu, B. Li, Z. Chen, J. Tse, S. Lu and B. Yang, *Adv. Mater.*, 2018, **30**, 1800676.
8 Z. Chen, C. Wu, Z. Zhang, W. Wu, X. Wang and Z. Yu, *Chin. Chem. Lett.*, 2018, **29**, 1601–1608.
9 P. Zhao, Q. Xu, J. Tao, Z. W. Jin, Y. Pan, C. M. Yu, *et al.*, Near infrared quantum dots in biomedical applications: current status and future perspective, *Wiley Interdiscip. Rev.: Nanomed. Nanobiotechnol.*, 2017, e1483.
10 J. K. Barton, E. D. Olmon and P. A. Sontz, *Coord. Chem. Rev.*, 2011, **255**, 619–634.
11 A. K. Geim and K. S. Novoselov, *Nat. Mater.*, 2007, **6**, 183–191.
12 J. Balapanuru, J. Yang, S. Xiao, Q. Bao, M. Jahan, L. Polavarapu, J. Wei, Q. Xu and K. P. Loh, *Angew. Chem., Int. Ed.*, 2010, **49**, 6549–6553.
13 T. Premkumar and K. E. Geckeler, *Prog. Polym. Sci.*, 2012, **37**, 515–529.
14 S. O. Kelley and J. K. Barton, *Science*, 1999, **283**, 375–381.
15 C. G. Pheeney and J. K. Barton, *J. Am. Chem. Soc.*, 2013, **135**, 14944–14947.
16 A. H. Castro Neto, F. Guinea, N. M. R. Peres, K. S. Novoselov and A. K. Geim, *Rev. Mod. Phys.*, 2009, **81**, 109–162.
17 F. Xia, T. Mueller, Y. Lin, A. Valdes-Garcia and P. Avouris, *Nat. Nanotechnol.*, 2009, **4**, 839–843.
18 A. Ambrosi and M. Pumera, *Phys. Chem. Chem. Phys.*, 2010, **12**, 8944–8948.

19 D. B. Hall, R. E. Holmlin and J. K. Barton, *Nature*, 1996, **382**, 731–735.
20 T. Rajh, Z. Saponjic, J. Q. Liu, N. M. Dimitrijevic, N. Scherer, F. M. Vega-Arroyo, P. Zapol, L. A. Curtiss and M. C. Thurnauer, *Nano Lett.*, 2004, **4**, 1017–1023.
21 C. Joachim, J. K. Gimzewski and A. Aviram, *Nature*, 2000, **408**, 541–548.
22 R. L. Carroll and C. B. Gorman, *Angew. Chem., Int. Ed.*, 2002, **41**, 4378–4400.
23 J. C. Genereux and J. K. Barton, *Nat. Chem.*, 2009, **1**, 106–107.
24 X. Guo, A. A. Gorodetsky, J. Hone, J. K. Barton and C. Nuckolls, *Nat. Nanotechnol.*, 2008, **3**, 163–167.
25 J. Jortner, M. Bixon, T. Langenbacher and M. E. Michel-Beyerle, *Proc. Natl. Acad. Sci. U. S. A.*, 1998, **95**, 12759–12765.
26 G. B. Schuster, *Acc. Chem. Res.*, 2000, **33**, 253–260.
27 E. M. Boon, D. M. Ceres, T. G. Drummond, M. G. Hill and J. K. Barton, *Nat. Biotechnol.*, 2000, **18**, 1096–1100.
28 K. E. Erkkila, D. T. Odom and J. K. Barton, *Chem. Rev.*, 1999, **99**, 2777–2795.
29 B. M. Zeglis, V. C. Pierre and J. K. Barton, *Chem. Commun.*, 2007, **44**, 4565–4579.
30 C. Hiort, P. Lincoln and B. Norden, *J. Am. Chem. Soc.*, 1993, **115**, 3448–3454.
31 A. M. Pyle, J. P. Rehmann, R. Meshoyrer, C. V. Kumar, N. J. Turro and J. K. Barton, *J. Am. Chem. Soc.*, 1989, **111**, 3051–3058.
32 X. Q. Lu, K. M. Zhu, M. Zhang, H. D. Liu and J. W. Kang, *J. Biochem. Biophys. Methods*, 2002, **52**, 189–200.
33 Z. Chang, J. Zhou, K. Zhao, N. Zhu, P. He and Y. Fang, *Electrochim. Acta*, 2006, **52**, 575–580.
34 T. Huang and R. W. Murray, *Langmuir*, 2002, **18**, 7077–7081.
35 H. Gorner, A. B. Tossi, C. Stradowski and D. Schultefrohlinde, *J. Photochem. Photobiol., B*, 1988, **2**, 67–89.
36 M. Eriksson, M. Leijon, C. Hiort, B. Norden and A. Graslund, *Biochemistry*, 1994, **33**, 5031–5040.
37 H. Y. Han, Z. K. He, E. E. Zeng and J. Fresen, *Anal. Chem.*, 1999, **364**, 782–785.
38 I. Haq, P. Lincoln, D. Suh, B. Norden, B. Z. Chowdhry and J. B. Chaires, *J. Am. Chem. Soc.*, 1995, **117**, 4788–4796.
39 K. F. Mårtensson, M. Abrahamsson, E. M. Tuite and P. Lincoln, *Inorg. Chem.*, 2019, **58**, 9452–9459.
40 V. Brabec and J. Kasparkova, *Coord. Chem. Rev.*, 2018, **376**, 75–94.
41 P. Lincoln, E. Tuite and B. Nordén, *J. Am. Chem. Soc.*, 1997, **119**, 1454–1455.
42 A. E. Friedman, J. C. Chambron, J. P. Sauvage, N. J. Turro and J. K. Barton, *J. Am. Chem. Soc.*, 1990, **112**, 4960–4962.
43 L. Hu, Z. Bian, H. Li, S. Han, Y. Yuan, L. Gao and G. Xu, *Anal. Chem.*, 2009, **81**, 9807–9811.
44 E. Treossi, M. Melucci, A. Liscio, M. Gazzano, P. Samori and V. Palermo, *J. Am. Chem. Soc.*, 2009, **131**, 15576–15577.
45 H. Dong, J. Zhang, H. Ju, H. Lu, S. Wang, S. Jin, K. Hao, H. Du and X. Zhang, *Anal. Chem.*, 2012, **84**, 4587–4593.
46 L. Sheng, J. Ren, Y. Miao, J. Wang and E. Wang, *Biosens. Bioelectronics*, 2011, **26**, 3494–3499.
47 Z. Qu, X. Zhou, L. Gu, R. Lan, D. Sun, D. Yu and G. Shi, *Chem. Commun.*, 2013, **49**, 9830–9832.
48 C. Zhu, S. Yang, J. Sun, P. He, N. Yuan, J. Ding, R. Mo, G. Wang, G. Ding and X. Xie, *Synth. Met.*, 2015, **209**, 468–472.
49 Z. Xu, J. Yu and G. Liu, *Sens. Actuators, B*, 2013, **181**, 209–214.
50 Y. Du, B. Qi, X. Yang and E. Wang, *J. Phys. Chem. B*, 2006, **110**, 21662–21666.
51 M. Zhao, N. Liao, Y. Zhuo, Y. Chai, J. Wang and R. Yuan, *Anal. Chem.*, 2015, **87**, 7602–7609.
52 J. Song, P. Amaladass, S. Wen, K. K. Pasunooti, A. Li, Y. Yu, X. Wang, W. Deng and X. Liu, *New J. Chem.*, 2011, **35**, 127–136.
53 K. Bhadra and G. S. Kumar, *Biochim. Biophys. Acta, Gen. Subj.*, 2011, **1810**, 485–496.
54 C. Wei, J. Wang and M. Zhang, *Biophys. Chem.*, 2010, **148**, 51–55.
55 J. Jaumot and R. Gargallo, *Curr. Pharm. Des.*, 2012, **18**, 1900–1916.
56 J. Liu, T. X. Zhang, T. B. Lu, L. H. Qu, H. Zhou, Q. L. Zhang and L. N. Ji, *J. Inorg. Biochem.*, 2002, **91**, 269–276.
57 G. Barone, C. F. Guerra, N. Gambino, A. Silvestri, A. Lauria, A. M. Almerico and F. M. Bickelhaupt, *J. Biomol. Struct. Dyn.*, 2008, **26**, 115–129.
58 P. Nagababu, D. A. Kumar, K. L. Reddy, K. A. Kumar, M. B. Mustafa, M. Shilpa and S. Satyanarayana, *Met.-Based Drugs*, 2008, 275084.
59 A. Schallon, C. V. Synatschke, D. V. Pergushov, V. Jerome, A. H. E. Mueller and R. Freitag, *Langmuir*, 2011, **27**, 12042–12051.
60 K. Huang, Z. Chen, Y. Liu, M. Wang, J. Wei, X. Xie, J. Zhang, K. Hu and H. Liang, *Eur. J. Med. Chem.*, 2013, **70**, 640–648.
61 M. Kaneko and C. Nagata, *Chem.-Biol. Interact.*, 1971, **3**, 459–468.
62 Z. Liu, Y. Si and X. Chen, *Acta Pharm. Sin. B*, 2010, **45**, 1478–1484.
63 J. Kypr, I. Kejnovska, D. Renciuk and M. Vorlickova, *Nucleic Acids Res.*, 2009, **37**, 1713–1725.
64 H. Qiu, J. B. Gilroy and I. Manners, *Chem. Commun.*, 2013, **49**, 42–44.
65 P. K. Yata, M. Shilpa, P. Nagababu, M. R. Reddy, L. R. Kotha, N. M. Gabra and S. Satyanarayana, *J. Fluoresc.*, 2012, **22**, 835–847.
66 S. T. Saito, G. Silva, C. Pungartnik and M. Brendel, *J. Photochem. Photobiol., B*, 2012, **111**, 59–63.
67 A. Kulkarni, S. A. Patil and P. S. Badami, *Eur. J. Med. Chem.*, 2009, **44**, 2904–2912.
68 R. Rastogi, N. Dhindsa, C. R. Suri, B. D. Pant, S. K. Tripathi, I. Kaur and L. M. Bharadwaj, *Mater. Chem. Phys.*, 2012, **135**, 268–276.
69 X. Wang, C. Ho, L. Yan, X. Chen, K. Cheung and W. Wong, *J. Inorg. Organomet. Polym.*, 2010, **20**, 478–487.
70 Q. Feng, N. Q. Li and Y. Y. Jiang, *Anal. Chim. Acta*, 1997, **344**, 97–104.
71 T. Dong, H. Lin, S. Lin, C. Huang, Y. Wen and L. Lee, *Organometallics*, 2008, **27**, 555–562.
72 X. Chu, G. L. Shen, J. H. Jiang, T. F. Kang, B. Xiong and R. Q. Yu, *Anal. Chim. Acta*, 1998, **373**, 29–38.

73 S. Shujha, A. Shah, Z. U. Rehman, N. Muhammad, S. Ali, R. Qureshi, N. Khalid and A. Meetsma, *Eur. J. Med. Chem.*, 2010, **45**, 2902–2911.
74 M. T. Carter and A. J. Bard, *J. Am. Chem. Soc.*, 1987, **109**, 7528–7530.
75 T. T. Williams, D. T. Odom and J. K. Barton, *J. Am. Chem. Soc.*, 2000, **122**, 9048–9049.
76 K. Hu, D. Lan, X. Li and S. Zhang, *Anal. Chem.*, 2008, **80**, 9124–9130.
77 M. Cho, S. Lee, S. Han, J. Park, M. A. Rahman, Y. Shim and C. Ban, *Nucleic Acids Res.*, 2006, **34**, 755–763.
78 Y. Ge, J. Wu, H. Ju and S. Wu, *Talanta*, 2014, **120**, 218–223.
79 Y. T. Long, C. Z. Li, T. C. Sutherland, M. Chahma, J. S. Lee and H. B. Kraatz, *J. Am. Chem. Soc.*, 2003, **125**, 8724–8725.
80 E. Wong and J. J. Gooding, *Anal. Chem.*, 2003, **75**, 3845–3852.
81 G. D. Hartwich, J. Caruana, T. de Lumley-Woodyear, Y. B. Wu, C. N. Campbell and A. Heller, *J. Am. Chem. Soc.*, 1999, **121**, 10803–10812.
82 Y. Osakada, K. Kawai, M. Fujitsuka and T. Majima, *Nucleic Acids Res.*, 2008, **36**, 5562–5570.
83 N. Kobayashi, S. Uemura, K. Kusabuka, T. Nakahira and H. Takahashi, *J. Mater. Chem.*, 2001, **11**, 1766–1768.
84 J. M. Kelly, A. B. Tossi, J. D. Mcconnell and C. Ohugin, *Nucleic Acids Res.*, 1985, **13**, 6017–6034.